The Cryosphere Discuss., 7, 3749–3781, 2013
www.the-cryosphere-discuss.net/7/3749/2013/
doi:10.5194/tcd-7-3749-2013

The Cryosphere Discussions
Open Access

Results from the DAMOCLES ice-buoy campaigns in the transpolar drift stream 2007–2009

M. Haller[1], B. Brümmer[2], and G. Müller[2]

[1]Helmholtz-Zentrum Geesthacht, Germany
[2]Meteorological Institute, University of Hamburg, Germany

Received: 18 May 2013 – Accepted: 1 July 2013 – Published: 24 July 2013

Correspondence to: B. Brümmer (burghard.bruemmer@zmaw.de)

Published by Copernicus Publications on behalf of the European Geosciences Union.

Abstract

During the EU research project DAMOCLES 18 ice buoys were deployed in the region of the Arctic transpolar drift (TPD). Sixteen of them formed a square with 400 km side-length. The measurements lasted from 2007 to 2009. The properties of the TPD and the impact of synoptic weather systems on the ice drift are analysed. Compared to Nansen's drift with the vessel Fram the measured speed of the TPD is here almost twice as fast. Within the TPD, the speed increases by a factor of almost three from the North Pole to the Fram Strait region. The hourly buoy position fixes show that the speed is underestimated by 10–20 % if positions were taken at only 1–3 days intervals as it is usually done for satellite drift estimates. The geostrophic wind factor U_i/U_g, i.e. the ratio of ice speed U_i and geostrophic wind speed U_g, in the TPD amounts to 0.012 on average, but with regional and seasonal differences. The constant U_i/U_g relation breaks down for $U_g < 5\,\mathrm{m\,s^{-1}}$. The impact of synoptic weather systems is studied applying a composite method. Cyclones (anticyclones) cause cyclonic (anticyclonic) vorticity and divergence (convergence) of the ice drift. The amplitudes are twice as large for cyclones as for anticyclones. The divergence caused by cyclones corresponds to a 0.1–0.5 %/6 h open water area increase based on the composite averages, but reached almost 4 % within one day during a strong August 2007 storm. This storm also caused a long-lasting (over several weeks) rise of U_i and U_i/U_g and changed the ice conditions in a way allowing ocean tidal motion to directly affect ice motion. The consequences of an increasing Arctic storm activity for the ice cover are discussed.

1 Introduction

The transpolar drift (TPD) is, together with the Beaufort gyre, one of the two large systems of sea-ice drift and near-surface currents in the Arctic Ocean. The TPD starts along the Siberian coast, progresses to the North Pole region, and ends in the Fram Strait. About 3000 km^3 of sea ice per year are transported with the TPD from the Arctic

Ocean into the North Atlantic. This corresponds to 15 % of the Arctic Ocean area if we assume an average ice thickness of 2 m. The ice export through Fram Strait shows large seasonal to inter-annual variations with amplitudes being about 50 % of the mean value (e.g. Affeld, 2003; Kwok et al., 2004). The speed of the TPD is also characterized by large variations showing high correlation with the east-west pressure gradient on the time scale of monthly to seasonal means (Vihma et al., 2012). The speed of the TPD in summer and the preceding winter affects the sea-ice extent minimum in the following September. A stronger TPD leads to a shorter stay of the sea ice in the Arctic Ocean and increases the ice export through Fram Strait. Smedsrud et al. (2011) showed that the recent (2004–2010) high sea ice area export in the Fram Strait contributed to the Arctic sea ice decline. A positive trend of the TPD speed for the period 1950–2006 was analysed by Hakkinen et al. (2008) using drift observations from the Russian North Pole stations, various expedition camps, and International Arctic Buoy Program (IABP). Gascard et al. (2008) have shown that the drift time of the French sailing vessel Tara from the Siberian side to Fram Strait in 2006–2007 was about half as long as the drift of the famous Norwegian vessel Fram in 1893–1896 for about the same distance.

The September ice extent minimum is mainly the integral result of the Fram Strait ice export and the summertime ice melt which depends on many factors such as the end-winter conditions of ice thickness and concentration, the ocean temperature, the solar insolation, which is closely related to cloud cover, and the warm-air advection from the surrounding land areas in summer. The latter are strongly controlled by synoptic pressure systems. For example, Screen et al. (2011) show that with more cyclonic activity in summer the sea ice is better protected from melting due to higher amount of clouds. On the other hand, cyclones cause a deformation of the ice and a decrease of ice concentration (Kriegsmann and Brümmer, 2013). In contrast to winter, the resulting openings remain open in summer and, thus, due to the positive albedo feedback, the ice melt can be increased. Furthermore, the decline of ice concentration reduces the internal forces and increases the mobility of the ice.

In this paper, we focus on the synoptic scale and investigate the impact of synoptic weather systems on the properties of the TPD. This is done by using data from an array of 16 ice buoys which were deployed in April 2007 around the above-mentioned French vessel Tara and data from two further buoys deployed in 2008. The measurements of the buoy array lasted until January 2008 and those of the other two buoys until 2009 and, thus, cover the period of the so far second-lowest ice extent minimum in September 2007 (the lowest occurred in September 2012). The experimental investigations aimed primarily at the following questions and so does our paper. (a) What are the kinematic properties of the TPD in the time range from hourly to seasonal? (b) How variable is the atmospheric dynamical forcing and what are the impacts of synoptic weather systems on the TPD? (c) What is the impact of a strong summer storm on the sea ice on the short and longer time scale?

The paper is organized along these questions. In Sect. 2 the buoys, their deployment, and the collected data are described. Section 3 deals with the kinematic properties of the TPD for different seasons and locations. In Sect. 4 the atmospheric wind forcing and the forcing–drift relation are investigated. Section 5 presents a composite study of the impact of cyclones and anticyclones on the vorticity, divergence and deformation of the ice drift and Sect. 6 deals with a case study of the strong summer storm on 13 August 2007 and its long-term consequences. A summary and conclusions are given in Sect. 7.

2 The DAMOCLES ice-buoy campaigns

In this study, we use data from two ice-buoy campaigns called here DAMOCLES 2007 (D07) and DAMOCLES 2008 (D08). Both field campaigns were operated by the Meteorological Institute of the University of Hamburg within the framework of the integrated project DAMOCLES (Developing Arctic Modelling and Observing Capabilities for Long-term Environmental Studies) which was funded by the European Commission.

TCD
7, 3749–3781, 2013

The D07 campaign used 16 CALIB (Compact Air-Launchable Ice Buoy) buoys manufactured by the Canadian company Metocean (Fig. 1). Buoys and data are described in a data publication (Brümmer et al., 2011a). The buoys were equipped with Alkali batteries for power supply, with a Vaisala PMB-100 pressure sensor and an YSI thermistor temperature sensor. The position was determined by the ARGOS satellite system with an accuracy of about 300 m. The buoy data were transmitted in irregular time intervals depending on the available satellite coverage. In the post-processing procedure the data were despiked and interpolated to regular 1 h intervals. The buoys were deployed in a regular quadratic grid of 400 km by 400 km side-length centred at the French sailing vessel Tara (see also Figs. 3 and 4) on 22 and 23 April 2007 with a Twinotter aircraft which could land and refuel on the ice near Tara. Since the buoys were dropped from the aircraft and landed uncontrolled, their exposure on the ice (ridge, trough, thin or thick ice, near a fracture) is unknown. This uncertainty makes it difficult to find out why the buoys were lost earlier or later. The buoy data availability is given in Fig. 2. The first buoy (no. 15) was lost already on 22 May 2007. In the following summer month further 13 buoys were temporarily lost, 6 of them recovered after some time. We are not sure what actually happened, but the Tara scientists reported a high fraction of melt ponds on the ice. This observation is supported by Rösel and Kaleschke (2012) who analysed from satellite data an exceptional melt pond occurrence in the Arctic in 2007. So, we assume that the buoys were partly submerged in the water, but could submit data again after summer when the melt ponds drained and disappeared. After all, 7 buoys survived the melting season. Out of these 7 buoys, only 3 buoys passed the Fram Strait in November/December 2007. The last buoy ended on 31 January 2008 near 70° N in the East-Greenland Current.

Within the D08 campaign 9 PAWS (Polar Area Weather Station) ice buoys also manufactured by the Canadian company Metocean were deployed (Fig. 1). PAWS and data are described in a data publication (Brümmer et al., 2011b). The PAWS were equipped with a Lithium battery for power supply, and with sensors for pressure, air temperature, ice temperature, relative humidity, and wind vector (Young). The position was determined via GPS and thus is accurate to about 10 m. The data were transmitted via Iridium at regular 3 hourly intervals (00, 03 ... UTC). The complex instrumentation of the PAWS required a manual installation on the ice. Seven of the PAWS, labelled A to G, were deployed between 12 and 22 April 2008 north of Ellesmere Island with the help of a Twinotter aircraft (7 flight missions) operating from Eureka airfield. Two further PAWS (H, I) were originally also planned to be deployed in that region, but did not work properly and, thus, had to be repaired by Metocean. They were deployed later by the German research vessel Polarstern, during the historically first cruise of a ship around the ice cap of the Arctic Ocean, on 21 September 2008 in the Beaufort Sea (H) and on 3 October 2008 in the Laptev Sea (I). In this paper, we use data only from the PAWS buoys G and I which moved with the TPD and reached the Fram Strait. The data availability is given in Fig. 2.The buoys measured until 18 July 2009 (G) and 23 February 2010 (I), thus, covering periods of more than one or even 2 yr, respectively.

The D07 campaign during the summer 2007 ice extent minimum took place around Tara which began its drift in September 2006 at about 79.8° N, 145° E not far north of the ice edge. Figure 3 shows the ice concentration on 1 May, 1 July, and 1 September 2007 together with the positions of the four corner buoys 1, 4, 13, and 16 of the D07 buoy square. The ice melt in 2007 which advanced northward beginning from the Beaufort Sea, Chukchi Sea, and East-Siberian Sea, fortunately did not reach the D07 buoy array, although on the satellite image for 1 July small areas with little ice concentration are discernible in that part of the buoy array where the first buoy (no.15) was lost. So, from the knowledge of the September 2006 ice edge which was close to Tara's drift start and the knowledge of the September 2007 ice edge it can be concluded that the ice melt in 2007 mainly concerned the new first year ice, but not all of it since the distance of Tara from the September 2007 ice edge was longer than its distance from the September 2006 ice edge.

TCD
7, 3749–3781, 2013

3 Drift characteristics

Figure 4 shows the drift of the D07 array and the PAWS G and I. Also shown is the drift of Tara from September 2006 until 23 April 2007. Afterwards, the Tara drift is not plotted because it forms the centre of the D07 array and the Tara drift is well represented e.g. by the buoy 11. Although with a time difference of 2 yr, Tara and I start in about the same region of the Arctic Ocean at about the same time of the year (October) and drift along a similar track in about the same time. In April 2009, PAWS I is almost in the same region where the D07 array started. PAWS G, further in the west of the TPD, begins its track one year later than the array and one year earlier than PAWS I, but at the same time of the year (April). The drift from May to September is similar to that of the array, but later it moves towards southwest and gets almost stuck from October 2008 to January 2009 in the very dense pack ice north of Greenland. Afterwards, G is again captured by the TPD and moves eastward north of the ice shear zone along the land-fast ice at the coast of North Greenland. Finally, G passes the Fram Strait (80° N) in March 2009, while I and the remaining buoys of the array (5, 11, and 16) pass 80° N about 3–4 months earlier.

Apart from the winter period when G got stuck in the pack ice north of Greenland, all buoys show an acceleration of the TPD from the region around the North Pole to the Fram Strait and the East-Greenland Current. This can be seen in the drift speed histograms for G, I, and the D07 buoys 5, 11, and 16 displayed in Fig. 5. The median values of drift speed (see Table 1) are around 7.5 $\mathrm{cm\,s^{-1}}$ in the region north of 85° N during the months May to September. The values increase in October and November further south, but still north of the Fram Strait, to median values around 13 $\mathrm{cm\,s^{-1}}$ and then accelerate in the Fram Strait and south of it to median values around 21 $\mathrm{cm\,s^{-1}}$. So the speed of the TPD increases by a factor of 2.7 from the North Pole to Fram Strait. The speed acceleration within the TPD is accompanied by a convergence of the ice drift towards Fram Strait as can be seen in Fig. 4.

TCD
7, 3749–3781, 2013

Results from the DAMOCLES ice-buoy campaigns

M. Haller et al.

Title Page
Abstract Introduction
Conclusions References
Tables Figures
Back Close
Full Screen / Esc
Printer-friendly Version
Interactive Discussion

Due to the influence of synoptic systems which is further detailed in Sects. 5 and 6, the buoy trajectories in the TPD show many curves and circles. Thus, when the position of an ice floe is taken at large time intervals e.g. of one or more days, as it is typically done for the estimation of ice drift from satellite data, the length of the trajectory and consequently the drift speed is underestimated. This is underlined in Fig. 6 showing the length of the trajectory calculated with different time steps. The speed underestimate is of the order of 10 % for 24 h intervals, of 20 % for 3-days intervals, and of 30–50 % for monthly time steps.

The area and the orientation of the D07 array show no monotonous variation with time. The array area increases slightly due to stretching of the lines 1–4 and 4–16, while 1–13 and 13–16 remain almost constant. The rotation is predominantly anticyclonic in May and June and changes to predominantly cyclonic from August until November. Also the variation of divergence and rotation is non-uniform for the various sub-areas. This is due to the fact that the entire array is rarely under the same atmospheric forcing. Passing lows and highs affect the different sub-areas in a different manner.

4 Drift–wind relation

The wind is the primary forcing for ice drift over time scales ranging from synoptic (e.g. Lammert et al., 2009; Brümmer et al., 2008) to climate (e.g. Vinje, 2001; Vihma et al., 2012). Figure 7 shows time series of ice drift U_{i}, geostrophic wind U_{g}, and geostrophic wind factor (ratio of U_{i} vs. U_{g}) for all buoys of the D07 array. The time step in Fig. 7 is 6 h because we calculated U_{g} from the sea-level pressure field of the operational ECMWF (European Centre for Medium-range Weather Forecast) analyses. Calculating U_{g} from the D07 buoy pressure field appeared to be too uncertain especially because 12 of the 16 buoys are edge buoys of the array. The ECMWF pressure field has a high degree of validity. The temporal pressure correlation between ECMWF and D07 buoys is higher than 0.99.

TCD
7, 3749–3781, 2013

U_i and U_g show a similar variation. Maxima of U_g always correspond to maxima of U_i. However, this is not true for the minima. The ratio U_i/U_g is 1.2 % on the average, spikes occur when U_g is low. The amplitudes of the U_i and U_i/U_g variations show a distinct step to higher values in August, although the amplitude of the U_g variations is almost the same from April to October 2007. This step is caused by a strong summer storm on 13 August 2007 as will be outlined in Sect. 6.

The relation between ice drift and geostrophic wind is displayed by U_i and the deviation angle $\alpha_i - \alpha_g$ as function of U_g in Fig. 8. Values of U_g reach up to $30\,\mathrm{m\,s^{-1}}$, the median is $7\,\mathrm{m\,s^{-1}}$. For values $U_g > 5\,\mathrm{m\,s^{-1}}$, an almost constant ratio of $U_i/U_g = 0.0115$ is present. For values $U_g < 5\,\mathrm{m\,s^{-1}}$, the ratio increases due to the inertia of the ice motion and the ocean current. The deviation angle $\alpha_i - \alpha_g$ is around 10° and shows no clear trend with U_g. The results, concerning U_i/U_g, fit well into the range of earlier studies (e.g. Thorndike and Colony, 1982), but disagree concerning $\alpha_i - \alpha_g$. Earlier studies indicate a higher deviation angle with decreasing U_g.

The ratio U_i/U_g and the deviation angle $\alpha_i - \alpha_g$ show a clear variation when distinguishing with respect to region and season as presented in Table 2. For this we have used monthly means from all data of the D07 array and the PAWS G and I. The regions Siberia (defined here as < 85° N, > 90° E) and North Pole (defined here as > 85° N) have a similar range of U_i/U_g values with minima < 1.0 % in late winter and maxima > 1.5 % in summer. The U_i/U_g values for buoy G in the dense pack ice north of Greenland are always < 1 % in autumn and winter. In contrast to that, the U_i/U_g values in the Fram Strait are the largest ones around 2 % even in winter. The deviation angle $\alpha_i - \alpha_g$ shows a distinct annual cycle in the regions Siberia/North Pole from 2° to 3° in winter to 14° to 18° in summer. In winter, the deviation angle is small (3° to 6°) north of Greenland and in the typical range (5° to 10°) in the Fram Strait region.

The ratio U_i/U_g and the angle difference $\alpha_i - \alpha_g$ depend on the local ice conditions (concentration, thickness) and, thus, on the relative magnitude of the internal forces. Ice conditions were even different within the comparatively small D07 array as can be

TCD
7, 3749–3781, 2013

Title Page
Abstract Introduction
Conclusions References
Tables Figures
◀ ▶
Back Close
Full Screen / Esc
Printer-friendly Version
Interactive Discussion

inferred from Table 3. In May/June, buoys 1–8 (see Fig. 4) have clearly larger U_i/U_g values than the other buoys in May/June. This gradient within the buoy array still exists in August/September, although the average U_i/U_g level in the array has increased from 1.09 % to 1.39 % between these two time periods.

5 Impact of synoptic systems: cyclones and anticyclones

In this section we analyse the impact of cyclones and anticyclones on vorticity, divergence, and deformation of the sea ice. Only data from the D07 array are used for this.

As an example, Fig. 9 shows the time series of vorticity, divergence, and deformation in the buoy triangle 3–10–16 together with the sea-level pressure measured at buoy 11 in the centre. An abrupt change of the amplitude of the vorticity, divergence, and deformation variations occurs with the passage of the 13 August storm. It can be seen that maxima and minima in the vorticity and divergence time series are mostly related with sea-level pressure extremes. Beside the impact of the particular characteristics of an individual synoptic system on the amplitude of the vorticity, divergence, and deformation variations, the amplitude depends also on the scale of the chosen triangle. The amplitude generally decreases with increasing scale (not shown).

To study the variation of vorticity, divergence, and deformation of the ice field in relation to synoptic systems in more detail but not for each individual system separately, we applied a composite method. Based on the 6 hourly ECMWF sea-level pressure analyses for the five-month period from May to September we selected 42 cases when a cyclonic system (low, trough or low-pressure line) and 32 cases when an anticyclonic system (high, ridge or bridge) passed over the D07 buoy array. During this period the centre of the array was always north of 85° N (see Figs. 3 and 4). Composites were calculated for a time window of 18 h centred at the system passage (t = 0 h) which we defined as the time when the vorticity attained its maximum (cyclonic system) or minimum (anticyclonic system). Composites were performed for 10 different triangles.

TCD
7, 3749–3781, 2013

Due to the many buoy losses in summer (see Fig. 2), for none of the triangles the full number of selected cases could be applied.

The results of the composites are shown in Fig. 10. The amplitude of the vorticity and divergence variations are roughly about twice as large for cyclonic as for anticyclonic systems. For cyclones, the vorticity is continuously positive within the time window. The largest maximum is found for the small triangle 2–3–8 and the smallest one for the large triangle 1–4–16. Converting vorticity to rotation rates, the composite cyclonic rotation of the ice field is $1.41^{\circ}/18\,\mathrm{h}$ for triangle 2–3–8 and $0.67^{\circ}/18\,\mathrm{h}$ for triangle 1–4–16. The peak composite rotation for triangle 2–3–8 is $0.14^{\circ}\,\mathrm{h}^{-1}$. The divergence composite for cyclones shows predominantly a divergent ice drift within the time window. It changes from weakly convergent before to clearly divergent after the passage. The average composite divergence during the first 6 h after the passage amounts between 0.05 and $0.25\ 10^{-6}\,\mathrm{s}^{-1}$ corresponding to a relative area increase i.e. area with new open water between 0.11 and $0.54\,\%/6\,\mathrm{h}$. The deformation shows less clear variation during the cyclone passage. A weak increase of deformation from negative to positive values is indicated around the passage time $t = 0\,\mathrm{h}$. Deformation is an additional process (in addition to divergence) to change ice concentration. Its effect is usually parameterized in numerical sea-ice models.

Why is the variation of divergence not symmetric with respect to cyclone passage ($t = 0$)? This is not obvious a priori. We propose the following possible explanation. We assume a rotationally symmetric cyclone which has a band of stronger wind around and weak wind in the centre. When the cyclone approaches the wind stress works on a not yet modified ice field and the ice starts to drift with an angle of about 10° to the right of the isobars, thus, leading to convergence. When the cyclone leaves the wind stress is basically the same, but now it works on an already modified ice field where the angle may be larger than 10° and where, in addition, the onset of an inertial oscillation caused by the just passed strong wind band may cause a further right-hand turning of the ice drift and thus leading to an ice drift divergence.

Passing anticyclonic weather systems cause a negative ice drift vorticity throughout the 18 h time window. The mean composite vorticity is $-0.15\ 10^{-6}\ \mathrm{s}^{-1}$ corresponding to a rotation rate of $-0.56^{\circ}/18\ \mathrm{h}$ averaged over all triangles. The time sequence of ice drift divergence during anticyclone passages is also asymmetric with respect to $t = 0$ and is opposite to that during cyclone passages. Divergence is around zero before the passage and changes to a distinct convergence afterwards. The largest convergence occurs 2–3 h after the passage. The overall impact of anticyclones is a convergent ice drift on the order of $-0.1\ 10^{-6}\ \mathrm{s}^{-1}$. The ice drift deformation shows a weak minimum around $t = 0$. In contrast to vorticity and divergence, the amplitude range of ice deformation values during anticyclone passages is the same as that during cyclone passages.

6 The storm of 13 August 2007

The composites in Sect. 5 have been calculated for all cyclones regardless of their amplitude. Single storms, however, can have by far larger amplitudes. The manifold consequences which a single strong storm can have, is demonstrated below with the summer storm passing the D07 array on 13 August 2007. Figure 11 shows the time series of drift speed U_i of all buoys in August. A distinct step-like increase of U_i occurs with the storm and U_i values remain high throughout August and even September. Not all buoys of the array were affected in the same way. Particularly buoys 2, 3, 4, and 8 in the "east" part of the array (see Fig. 4) show periodic oscillations which continue for several weeks. The mean period of the oscillations between 13 and 20 August is close to 12 h. Both, the buoy trajectories and the ice velocity hodographs show a right-hand turning of the ice drift. It cannot be distinguished whether the oscillation is of inertial or tidal origin since both have almost identical periods. The weeks-long duration of the oscillations speaks more for a tidal oscillation. Thus, the storm modified the ice conditions within a sub-area of the array (the same sub-area in which already in May/June the largest $U_\mathrm{i}/U_\mathrm{g}$ ratios were found, see Table 3) in a way allowing the ocean tidal mo-

TCD
7, 3749–3781, 2013

tion now to fully affect the motion of the ice cover. Table 4 shows the spatial distribution of the oscillation amplitude averaged over the period 13–20 August. The highest double amplitude with 16.2 $\mathrm{cm\,s^{-1}}$ was measured at buoys 2 and 3. The maximum ice speed during the storm passage amounted to 0.53 $\mathrm{m\,s^{-1}}$ at buoy 3. This is a large value for the TPD in the North Pole region (the median value there is 7.5 $\mathrm{cm\,s^{-1}}$) and is otherwise observed only at the ice edge or in the Fram Strait.

The area change corresponding to the divergence caused by the storm for the 24 h period from 12:00 UTC on 12 August to 12:00 UTC on 13 August is between 0.1 and 3.6 % depending on the sub-area. This is the integral storm effect; superimposed on this are oscillations of divergence and vorticity due to the oscillating ice motion. Table 5 shows maxima and minima of divergence and vorticity for some triangles of the array occurring during the oscillations on 13 August. Instantaneous divergence maxima during the oscillation amount to 4 times the integral 24 h divergence. The peak values for divergence are 1.67 $10^{-6}\,\mathrm{s^{-1}}$ (corresponding to an area change of 0.6 $\%\,\mathrm{h^{-1}}$) in triangle 2–3–10 and those for vorticity are 2.67 $10^{-6}\,\mathrm{s^{-1}}$ (corresponding to a rotation rate of 0.55$^\circ\,\mathrm{h^{-1}}$). The minimum values of divergence and vorticity during the oscillation have negative signs but are absolutely smaller so that the above-mentioned integral effect remains. Opening and closing of the ice deck during the oscillation cycle does not return to the initial state of the ice field. It is an irreversible process.

7 Summary and conclusions

Within the DAMOCLES research project 18 ice buoys were deployed in the region of the TPD. Sixteen of them formed a square of 400 km side-length. The measurements covered the period 2007–2009. The data were used to analyse the properties of the TPD and the impact of synoptic weather systems on the ice drift.

Compared to earlier studies (e.g. Gascard et al., 2008; Hakkinen et al., 2008), our measurements also show that the TPD was almost twice as fast as hundred years ago during the drift of Norwegian vessel Fram. Within the TPD we find an increase of the drift speed by a factor of almost 3 from the North Pole region towards Fram Strait. The high temporal resolution (1–3 h) of the buoy position fixes shows that the TPD is subjected to many detours manifested as curves and circles caused by passing weather systems. If the positions were taken at only 1–3 days intervals as it is typically done for satellite drift estimates, the drift speed is underestimated by 10–20 %.

The overall geostrophic wind factor U_i/U_g in the TPD amounts to 0.012, however, with regional and seasonal differences. The smallest values occur north of Greenland, the largest ones in the Fram Strait. Wind factor values are larger in summer than in winter as was also found by other authors (e.g. Thorndike and Colony, 1982; Kimura and Wakatsuchi, 2000). A distinct deviation from the above-mentioned wind factor to higher values occurs for $U_g < 5\,\mathrm{m\,s^{-1}}$ as was also found by e.g. Thorndike and Colony (1982). In contrast to these studies, we find no change of the deviation angle $\alpha_i - \alpha_g$ with U_g. A gradient of U_i/U_g was present within the buoy array at the beginning of the field experiment and still existed five months later. This demonstrates that characteristics of the ice cover have a long lifetime.

The influence of synoptic weather systems on the sea ice was studied applying a composite method. Cyclonic weather systems cause cyclonic vorticity and divergence whereas anticyclonic systems cause anticyclonic vorticity and convergence of the ice drift. The amplitude of the variations is about twice as large for cyclones as for anticyclones. The temporal evolution of divergence is asymmetric with respect to the passage time. Maximum values of divergence (convergence) occur after the cyclone (anticyclone) passage. Typical divergence values are 0.1–0.5 %/6 h indicating the generation of open water areas. Causes for the asymmetry are not exactly understood, but probably are related to the fact that the approaching (leaving) system works on yet unmodified (already modified) ice field.

A strong summer storm caused a step-like rise of drift speed which remained over several weeks. In addition, the ice cover was modified in such a way that the tidal motion affects directly the ice motion, also remaining over several months. The storm-related divergence caused an increase of open water areas of up to 3.6 % in some parts of the array.

Following the studies of an increased cyclone frequency in the Arctic (e.g. Affeld, 2003; Zhang et al., 2004; Serreze and Barrett, 2008; Haller, 2011) and combining them with our results, this must have been accompanied by an increased ice drift divergence and by corresponding, already in the introduction mentioned different consequences in summer (more ice melt) and winter (more ice formation). Whether the observed long-term acceleration of the speed of the TPD is more a direct consequence of the increased cyclone activity and thus a higher surface stress or whether it is more an indirect consequence of the cyclone-related ice divergence and thus a smaller internal ice stress cannot be answered here, but is an open scientific issue. For the period 2001–2009, Kwok et al. (2013) found large spatially averaged drift speed trends of about 20 % per decade but much smaller wind speed trends. This underlines the importance of the indirect effect of the wind forcing which is to reduce the internal ice stress.

On the other hand, our measurements also show that already a single storm, if exceeding certain thresholds, can have long-term consequences for the ice cover (at least in summer). Perovich et al. (2012) also mentioned that a severe storm in August 2012 (the year with the latest record ice extent minimum in September) accelerated the ice loss in the Pacific Arctic. Exceeding of thresholds includes both, i.e. thresholds of the atmospheric forcing and thresholds of the properties of the ice deck. Because of the non-linearity implied by these thresholds the simulation and prognosis of the Arctic ice cover remains a sensitive task.

Acknowledgements. This paper has received support by the integrated research project DAMOCLES within the EU 6th framework programme.

The service charges for this open access publication
have been covered by a Research Centre of the
Helmholtz Association.

TCD
7, 3749–3781, 2013

References

Affeld, B.: Zyklonen in der Arktis und ihre Bedeutung für den Eistransport durch die Framstraße, Ph.D thesis, University Hamburg, Germany, 125 pp., 2003.

Brümmer, B., Schröder, D., Müller, G., Spreen, G., Jahnke-Bornemann, A., and Launiainen, J.: Impact of a Fram Strait cyclone on ice edge, drift, divergence, and concentration: possibilities and limits of an observational analysis. J. Geophys. Res., 113, C12003, doi:10.1029/2007JC004149, 2008.

Brümmer, B., Müller, G., Haller, M., Kriegsmann, A., Offermann, M., and Wetzel, C.: DAMOCLES 2007–2008 – Hamburg Arctic Ocean buoy drift experiment: meteorological measurements of 16 autonomous drifting ice buoys, doi:10.1594/WDCC/UNI_HH_MI_DAMOCLES2007, 2011a.

Brümmer, B., Müller, G., Haller, M., Kriegsmann, A., Offermann, M., and Wetzel, C.: DAMOCLES 2008–2011 – Hamburg Arctic Ocean buoy drift experiment: meteorological measurements of 9 autonomous drifting ice buoys, doi:10.1594/WDCC/UNI_HH_MI_DAMOCLES2008, 2011b.

Gascard, J.-C., Festy, J., Le Goff, H., Weber, M., Brümmer, B., Offermann, M., Doble, M., Wadhams, P., Forsberg, R., Hanson, S., Skourup, S., Gerland, S., Nicolaus, M., Metaxian, J.-P., Grangeon, J., Haapala, J., Rinne, E., Haas, C., Heygster, G., Jacobson, E., Palo, T., Wilkinson, J., Kaleschke, L., Claffey, K., Elder, B., and Bottenheim, J.: Exploring Arctic transpolar drift during dramatic sea ice retreat, EOS, Transactions, 89, 21–28, 2008.

Hakkinen, S., Proshutinsky, A., and Ashik, I.: Sea ice drift in the Arctic since the 1950s, Geophys. Res. Lett., 35, L19704, doi:10.1029/2008GL034791, 2008.

Haller, M.: Arktische Zyklonen und Meereeisdrift während der DAMOCLES-Bojenexperimente 2007–2010, Ph.D thesis, University Hamburg, Germany, 201 pp., 2011.

Kimura, N. and Wakatsuchi, M.: Relationship between sea-ice motion and geostrophic wind in the Northern Hemisphere, Geophys. Res. Lett., 27, 3735–3738, 2000.

Kriegsmann, A. and Brümmer, B.: Cyclone impact on sea ice in the central Arctic Ocean: a statistical study,The Cryosphere Discuss., 7, 1141–1176, doi:10.5194/tcd-7-1141-2013, 2013

Kwok, R., Cunningham, G. F., and Pang, S. S.: Fram Strait sea ice outflow, J. Geophys. Res., 109, C01009, doi:10.1029/2003JC001785, 2004.

Kwok, R., Spreen, G., and Pang, S.: Arctic sea ice circulation and drift speed: decadal trends and ocean currents, J. Geophys. Res.-Oceans, 118, 2408–2425, doi:10.1002/jgrc.20191, 2013.
Lammert, A., Brümmer, B., and Kaleschke, L.: Observation of cyclone-induced inertial sea-ice oscillation in Fram Strait, Geophys. Res. Lett., 36, L10503, doi:10.1029/2009GL037197, 2009.
Perovich, D., Meier, W., Tschudi, M., Gerland, S., and Richter-Menge, J.: Sea ice, in: Arctic Report Card 2012, http://www.arctic.noaa.gov/reportcard, 37–42, 2012.
Rösel A., and Kaleschke, L.: Exceptional melt pond occurrence in the years 2007 and 2011 on the Arctic sea ice revealed from MODIS satellite data, J. Geophys. Res., 117, C05018, doi:10.1029/2011JC007869, 2012.
Screen, J. A., Simmonds, I., and Keay, K.: Dramatic interannual changes of perennual Arctic sea ice linked to abnormal summer storm activity, J. Geophys. Res.-Atmos., 116, D15105, doi:10.1029/2011JD015847, 2011.
Serreze, M. C. and Barnett, A. P.: The summer cyclone maximum over the central Arctic Ocean, J. Climate, 21, 1048–1065, 2008.
Smedsrud, L. H., Sirevaag, A., Kloster, K., Sorteberg, A., and Sandven, S.: Recent wind driven high sea ice area export in the Fram Strait contributes to Arctic sea ice decline, The Cryosphere, 5, 821–829, doi:10.5194/tc-5-821-2011, 2011.
Thorndike, A. S. and R. Colony: Sea ice motion in response to geostrophic winds, J. Geophys. Res., 87, 5845–5852, 1982.
Vihma, T., Tisler, P., and Uotila, P.: Atmospheric forcing on the drift of Arctic sea ice in 1989–2009, Geophys. Res. Lett., 39, L02501, doi:10.1029/2011GL050118, 2012.
Vinje, T.: Fram Strait ice fluxes and atmospheric circulation 1950–2000, J. Climate, 14, 3508–3517, 2001.
Zhang, X., Walsh, J., Zhang, J., Bhatt, U., and Ikeda, M.: Climatology and interannual variability of Arctic cyclone activity, J. Climate, 17, 2300–2317, 2004.

Table 1. Median values of drift speed in $\mathrm{cm\,s^{-1}}$ for five buoys in different regions of the transpolar drift stream.

Buoy	> 85° N (May–Sep)	85° N – Fram Strait (Oct–Nov)	Fram Strait (Dec–Jan)
5	6.5	12	18
11	7.5	11	22.5
16	7	16	–
G	7	4	10
I	9	13	21.5
Mean (without G)	$7.5\,\mathrm{cm\,s^{-1}}$	$13.0\,\mathrm{cm\,s^{-1}}$	$20.7\,\mathrm{cm\,s^{-1}}$

TCD
7, 3749–3781, 2013

TCD
7, 3749–3781, 2013

Table 2. Monthly averages of U_i/U_g in % and difference angle $\alpha_i - \alpha_g$ in four regions of the transpolar ice drift based on data from the D07 array and the PAWS buoys G and I.

Month	J	F	M	A	M	J	J	A	S	O	N	D	Source
Siberia	1.15 1°	0.95 −2°	0.80 −3°	1.12 4°						1.45 10°	1.20 5°	1.10 2°	I
North Pole					1.04 14°	1.08 17°	1.58 17°	1.45 18°	1.30 ?				Array, G, I
Greenland										0.85 3°	0.89 6°	0.94 4°	G
Fram Strait			1.80 10°									2.20 5°	G, I

Table 3. Average ratios of U_i/U_g in % during the periods May/June and August/September 2007 for all 16 D07 ice buoys.

Buoy no.	1	2	3	4	5	6	7	8	9	10	11	12	13	14	15	16
May/Jun	1.43	1.27	1.18	1.17	1.25	1.14	1.06	1.12	0.91	1.18	0.95	0.96	0.91	0.98	0.82	1.08
Aug/Sep	1.47	1.36	1.82	–	1.12	–	–	1.44	–	1.55	1.21	–	–	–	–	1.11

TCD
7, 3749–3781, 2013

Table 4. Mean double amplitude of ice drift oscillations in $cm\,s^{-1}$ in the D07 buoy array during the one-week period 13 and 19 August after the cyclone passage on 13 August.

Buoy no.	1	2	3	4	5	6	7	8	9	10	11	12	13	14	15	16
$cm\,s^{-1}$	7.9	16.2	16.2	–	6.3	–	–	15.0	–	5.1	9.8	–	–	–	–	7.7

TCD
7, 3749–3781, 2013

Results from the DAMOCLES ice-buoy campaigns

M. Haller et al.

Table 5. Maxima and minima of ice drift divergence and vorticity oscillations on 13 August 2007 for 8 triangles of the D07 buoy array.

Triangle	Divergence in $10^{-6}\,s^{-1}$		Vorticity in $10^{-6}\,s^{-1}$	
	Max	Min	Max	Min
02–03–10	1.67	−1.67	1.93	−1.47
02–03–08	1.47	−2.00	2.67	−1.33
02–05–10	0.67	−0.47	0.93	−0.40
02–03–11	1.07	−1.33	2.00	−0.73
03–10–16	0.47	−0.27	1.00	−0.53
03–08–11	1.33	−0.80	2.00	−0.73
01–02–05	0.53	−0.53	1.07	−0.80
02–05–16	0.80	−0.67	0.93	−0.93

TCD
7, 3749–3781, 2013

Fig. 1. Top: CALIB buoy dropped from Twinotter aircraft at 300 m altitude and descending on parachute. Bottom: PAWS buoy G after installation with Twinotter aircraft landed on ice.

TCD
7, 3749–3781, 2013

Results from the DAMOCLES ice-buoy campaigns

M. Haller et al.

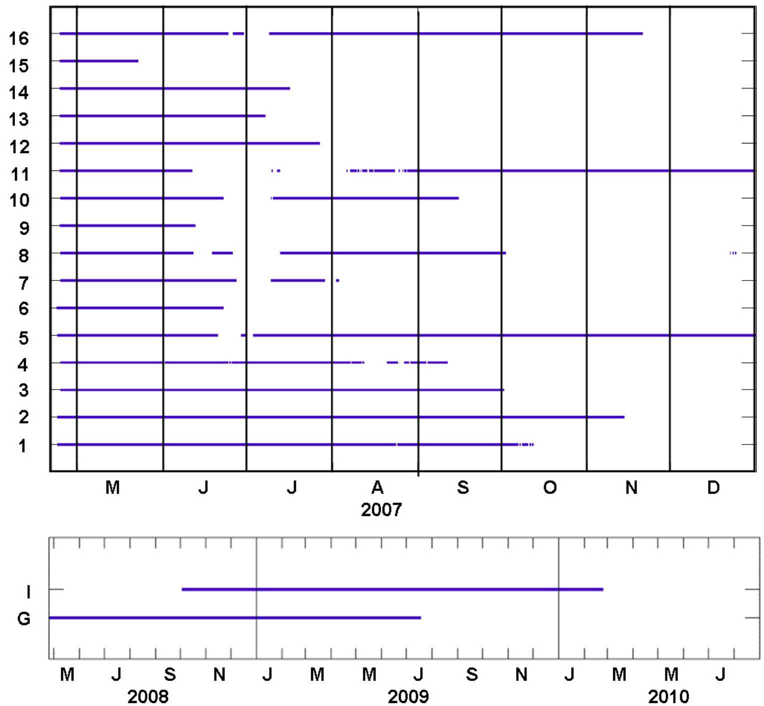

Fig. 2. Data availability of all 16 CALIB buoys in 2007 (top) and of PAWS buoys G, I in 2008–2010 (below).

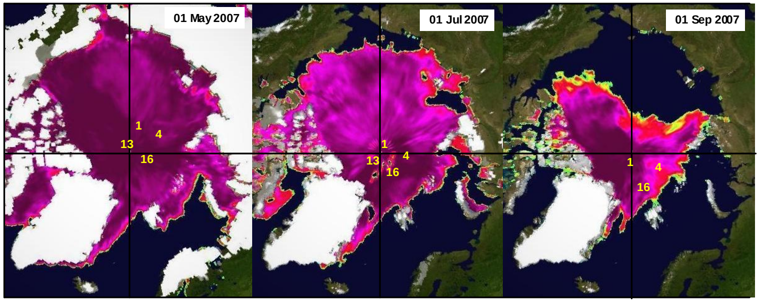

Fig. 3. Ice extent and concentration on 1 May, 1 July, and 1 September 2007 (from The Cryosphere Today) together with location of the four corner buoys 1, 4, 13, and 16 of the D07 buoy array.

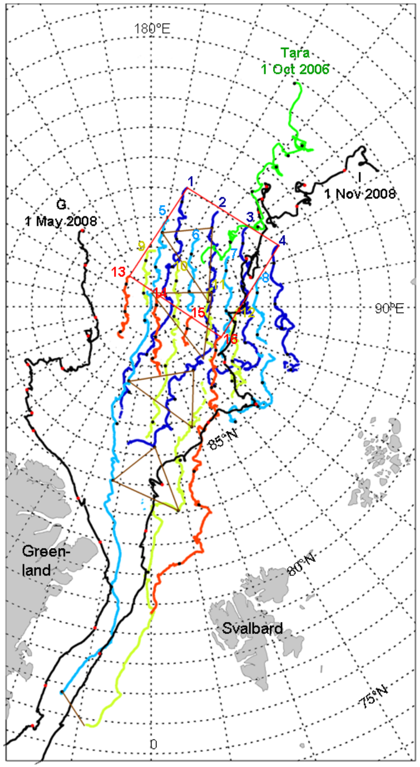

Fig. 4. Drift trajectories of all 16 D07 CALIB buoys, the French sailing vessel Tara (green), and the D08 PAWS buoys G and I (black). Dot marks position on first day of month. Red square surrounds the D07 buoy array at the beginning on 24 April 2007. For a better visualisation of the ice motion the position of the buoy triangle 2–5-11 is given in 2-months intervals on 1 May, 1 July, 1 September, and 1 November 2007. Only the line 5–11 of the triangle is left on 1 January 2008.

TCD

7, 3749–3781, 2013

Results from the DAMOCLES ice-buoy campaigns

M. Haller et al.

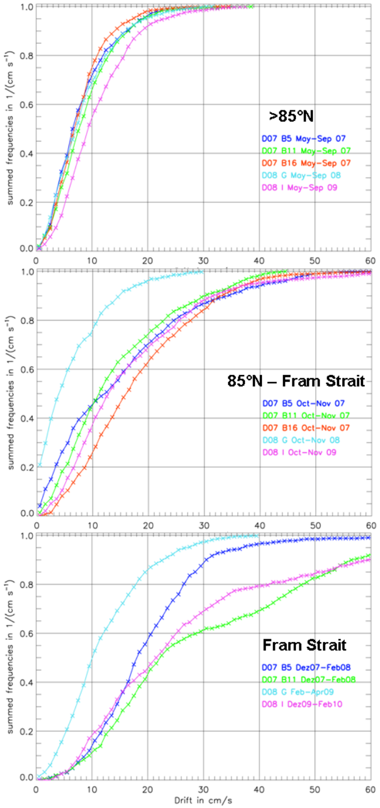

Fig. 5. Histograms of drift velocity for D07 buoys 5, 11, 16 and D08 buoys G, I for different regions of the transpolar drift. Note that the curves hold for different years.

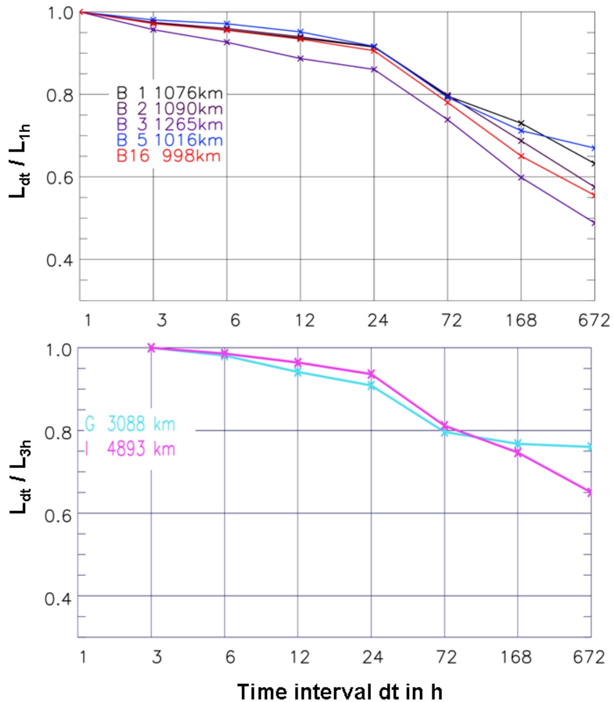

Fig. 6. Normalized length of ice drift trajectories calculated with different time intervals. The length is normalized by the length (given in the figure) calculated with the shortest time interval which is 1 h for the CALIB buoys (above) and 3 h for the PAWS buoys (below).

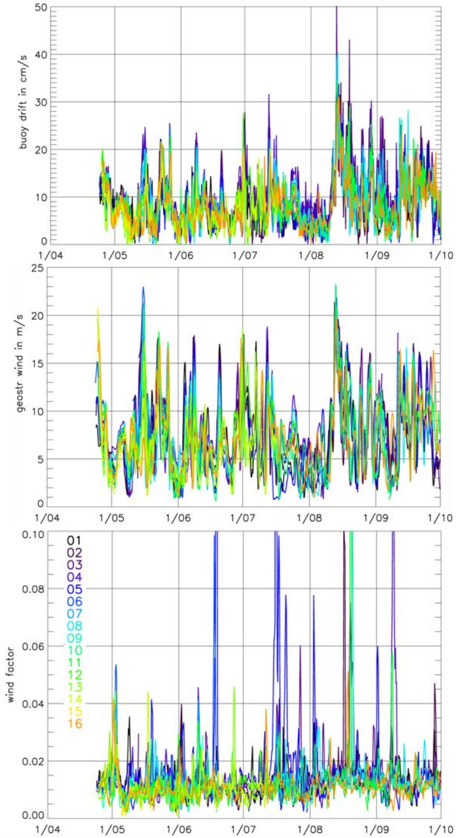

Fig. 7. Time series of 6 hourly ice drift (top), geostrophic wind (middle), and geostrophic wind factor (bottom) for all buoys of the D07 array.

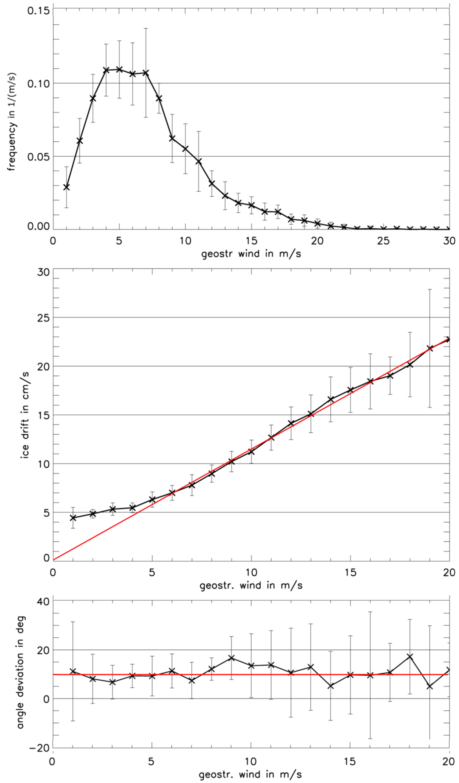

Fig. 8. Frequency distribution of geostrophic wind (top) and variation of magnitude of ice drift velocity (middle) and angle between ice velocity and geostrophic wind (bottom) for various magnitudes of the geostrophic wind based on all 16 Damocles 2007 buoys for the period 01 May to 30 September 2007.

TCD
7, 3749–3781, 2013

Results from the DAMOCLES ice-buoy campaigns

M. Haller et al.

Title Page
Abstract
Introduction
Conclusions
References
Tables
Figures
◀I
▶I
◀
▶
Back
Close
Full Screen / Esc
Printer-friendly Version
Interactive Discussion

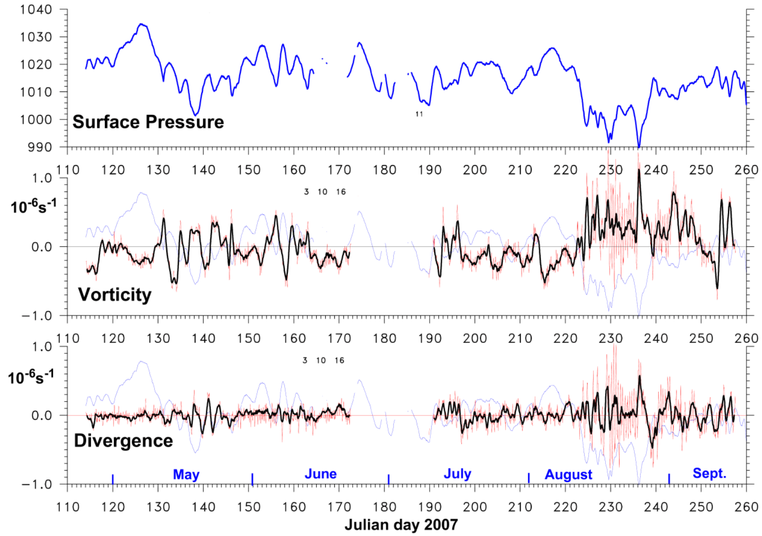

Fig. 9. Time series of ice drift vorticity and divergence in the D07 buoy triangle 03–10-16 with 2 h resolution (red) and as 12 h running mean (black) together with the sea-level pressure at buoy 11 in the middle of the triangle. To ease visual correlation the pressure is repeated as thin curve in the vorticity and divergence panels.

TCD
7, 3749–3781, 2013

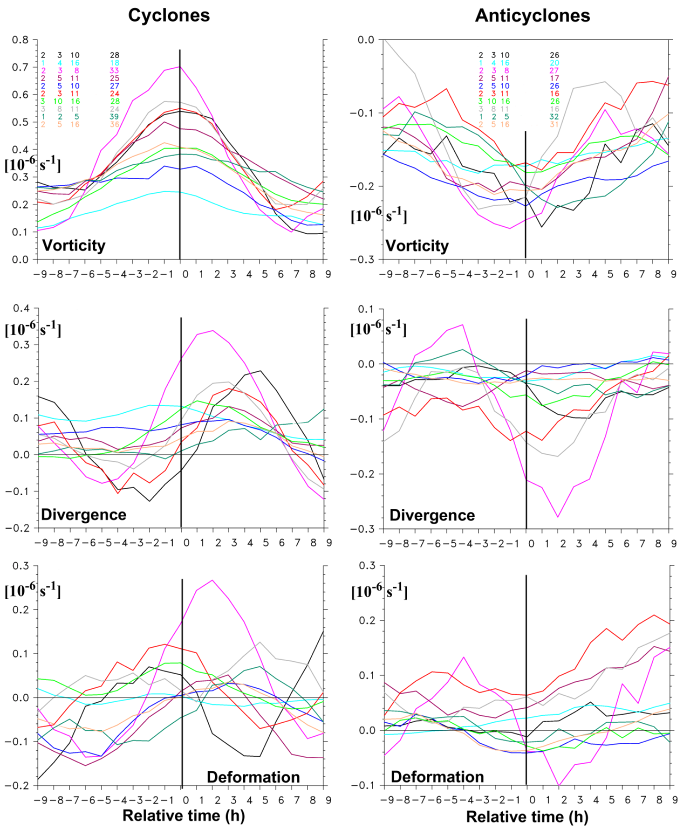

Fig. 10. Composite time development of ice drift vorticity, divergence and deformation for 10 different triangles within the D07 buoy array during cyclone (left) and anticyclone (right) passages. The time is relative to the vorticity maximum (minimum). The number of cases used for each triangle composite is listed in the upper panels. Note the different scales for cyclones and anticyclones.

TCD
7, 3749–3781, 2013

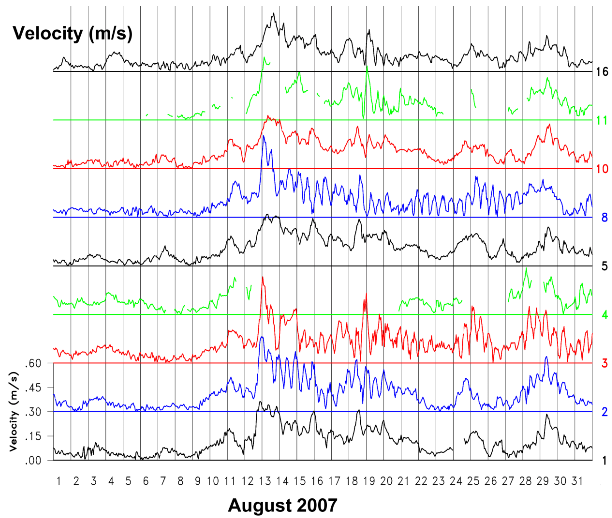

Fig. 11. Time series of hourly ice drift magnitude in the D07 buoy array during August 2007. A different ice drift regime begins with the storm on 13 August.

TCD
7, 3749–3781, 2013